Dysregulation of the NRG1/ERBB pathway causes a developmental disorder with gastrointestinal dysmotility in humans

Thuy-Linh Le,[1] Louise Galmiche,[2,3] Jonathan Levy,[4,5] Pim Suwannarat,[6] Debby M.E.I. Hellebrekers,[7] Khomgrit Morarach,[8] Franck Boismoreau,[9] Tom E.J. Theunissen,[10] Mathilde Lefebvre,[11] Anna Pelet,[1] Jelena Martinovic,[12] Antoinette Gelot,[13,14] Fabien Guimiot,[5,15] Amanda Calleroz,[16] Cyril Gitiaux,[17] Marie Hully,[18] Olivier Goulet,[19] Christophe Chardot,[20] Severine Drunat,[4,5] Yline Capri,[4] Christine Bole-Feysot,[21] Patrick Nitschké,[22] Sandra Whalen,[23] Linda Mouthon,[24] Holly E. Babcock,[25] Robert Hofstra,[26] Irenaeus F.M. de Coo,[27] Anne-Claude Tabet,[4,28] Thierry J. Molina,[3,29] Boris Keren,[24] Alice Brooks,[26] Hubert J.M. Smeets,[27] Ulrika Marklund,[8] Christopher T. Gordon,[1] Stanislas Lyonnet,[1,30] Jeanne Amiel,[1,30] and Nadège Bondurand[1]

[1]Laboratory of Embryology and Genetics of Human Malformation, Imagine Institute, INSERM UMR 1163, Université de Paris, Paris, France. [2]INSERM UMR 1235, TENS, The Enteric Nervous System in Gut and Brain Diseases, IMAD, University of Nantes, Nantes, France. [3]Pathology Department, Assistance Publique Hôpitaux de Paris (AP-HP), Necker-Enfants Malades Hospital, Paris, France. [4]Genetics Department, Robert Debré Hospital, AP-HP, Paris, France. [5]Université de Paris, NeuroDiderot, INSERM UMR 1141, Paris, France. [6]Department of Genetics, Mid-Atlantic Permanente Medical Group, Suitland, Maryland, USA. [7]Department of Clinical Genetics, Maastricht University Medical Center, Maastricht, Netherlands. [8]Division of Molecular Neurobiology, Department of Medical Biochemistry and Biophysics, Karolinska Institutet, Stockholm, Sweden. [9]Institut de Biologie de l'ENS (IBENS), INSERM, CNRS, École Normale Supérieure, PSL Research University, Paris, France. [10]Department of Genetics and Cell Biology, Maastricht University, Maastricht, Netherlands. [11]Fetal Pathology Unit, Armand Trousseau Hospital, AP-HP, Paris, France. [12]Fetal Pathology Unit, Antoine Béclère Hospital, AP-HP, Paris-Saclay University, Clamart, France. [13]Neuropathology, Pathology Department, Armand Trousseau Hospital, AP-HP, Paris, France. [14]Aix-Marseille University, INMED INSERM UMR1249, Campus de Luminy, Marseille, France. [15]Fetal Pathology Unit, Robert Debré Hospital, AP-HP, Paris, France. [16]Pathology and Laboratory Medicine Division, Children's National Hospital, Washington DC, USA. [17]Department of Pediatric Clinical Neurophysiology, Necker-Enfants Malades Hospital, AP-HP, Université de Paris, Paris, France. [18]Department of Pediatric Neurology and Rehabilitation, Necker-Enfants Malades Hospital, AP-HP, Université de Paris, Paris, France. [19]Department of Pediatric Gastroenterology-Hepatology-Nutrition, Necker-Enfants Malades Hospital, AP-HP, Paris, France. [20]Department of Pediatric Surgery, Necker-Enfants Malades Hospital, AP-HP, Paris, France. [21]Genomics Core Facility, Imagine Institute-Structure Federative de Recherche Necker, INSERM UMR 1163 and INSERM US24/CNRS UMS 3633, Université de Paris, Paris, France. [22]Bioinformatics Platform, Imagine Institute, Paris, France. [23]Clinical Genetics Unit and Reference Center, Anomalies du Développement et Syndromes Malformatifs, AP-HP, Sorbonne University, Armand Trousseau Hospital, Paris, France. [24]Department of Genetics, La Pitié-Salpêtrière Hospital, AP-HP, Paris, France. [25]Children's National Hospital, Rare Disease Institute, Washington, DC, USA. [26]Department of Clinical Genetics, Erasmus Medical Center, Rotterdam, Netherlands. [27]Department of Toxicogenomics, Unit Clinical Genomics, Maastricht University, MHeNs School for Mental Health and Neuroscience, Maastricht, Netherlands. [28]Human Genetics and Cognitive Functions, Institut Pasteur, UMR3571 CNRS, Université de Paris, Paris, France. [29]Université de Paris, Imagine Institute, Laboratory of Molecular Mechanisms of Hematological Disorders and Therapeutic Implications, INSERM UMR 1163, Paris, France. [30]Fédération de Génétique, Necker-Enfants Malades Hospital, AP-HP, Paris, France.

Hirschsprung disease (HSCR) is the most frequent developmental anomaly of the enteric nervous system, with an incidence of 1 in 5000 live births. Chronic intestinal pseudo-obstruction (CIPO) is less frequent and classified as neurogenic or myogenic. Isolated HSCR has an oligogenic inheritance with *RET* as the major disease-causing gene, while CIPO is genetically heterogeneous, caused by mutations in smooth muscle–specific genes. Here, we describe a series of patients with developmental disorders including gastrointestinal dysmotility, and investigate the underlying molecular bases. Trio-exome sequencing led to the identification of biallelic variants in *ERBB3* and *ERBB2* in 8 individuals variably associating HSCR, CIPO, peripheral neuropathy, and arthrogryposis. Thorough gut histology revealed aganglionosis, hypoganglionosis, and intestinal smooth muscle abnormalities. The cell type–specific *ErbB3* and *ErbB2* function was further analyzed in mouse single-cell RNA sequencing data and in a conditional *ErbB3*-deficient mouse model, revealing a primary role for *ERBB3* in enteric progenitors. The consequences of the identified variants were evaluated using quantitative real-time PCR (RT-qPCR) on patient-derived fibroblasts or immunoblot assays on Neuro-2a cells overexpressing WT or mutant proteins, revealing either decreased expression or altered phosphorylation of the mutant receptors. Our results demonstrate that dysregulation of ERBB3 or ERBB2 leads to a broad spectrum of developmental anomalies, including intestinal dysmotility.

▶ **Related Commentary: https://doi.org/10.1172/JCI146389**

Authorship note: JL, PS, and DMEIH contributed equally to this work. JA and NB contributed equally to this work.
Conflict of interest: The authors have declared that no conflict of interest exists.

Submitted: November 9, 2020; **Accepted:** January 14, 2021; **Published:** March 15, 2021.
Reference information: *J Clin Invest*. 2021;131(6):e145837. https://doi.org/10.1172/JCI145837.

Introduction

Neurocristopathies are developmental disorders and cancers that arise from defects of neural crest development. Hirschsprung disease (HSCR, aganglionic megacolon, OMIM 142623) is a neurocristopathy and is the most frequent cause of intestinal obstruction with an incidence of 1/5000 live births (1–3). HSCR is characterized by the absence of intrinsic ganglion cells in the submucosal and myenteric plexuses over a variable length of the distal part of the gut (4). HSCR is either isolated or associated with other malformations (syndromic HSCR) in about 80% and 20% of cases, respectively (2).

Hitherto, known HSCR-associated genes accounted for approximately 60% of cases (3). Isolated HSCR has an oligogenic, sex-dependent mode of inheritance, with mutations in *RET* being the major cause. Vertical transmission of rare loss-of-function *RET* variants occurs in about 50% of familial cases, and low-penetrance noncoding variants at the *RET* locus have been associated with HSCR (5–10). Several monogenic syndromes with a variable predisposition to HSCR, including those associated with variants in *ZEB2*, *EDNRB*, *EDN3*, *PHOX2B*, and *SOX10,* have been delineated (2). However, many patients presenting syndromic HSCR remain without a molecular diagnosis, with consequences on clinical management and genetic counseling.

Apart from HSCR, other gut dysmotility disorders are hypoganglionosis and chronic intestinal pseudo-obstruction (CIPO). The latter is characterized by continuous or episodic bowel obstruction without evidence of mechanical occlusion, and is classified as myogenic or neurogenic (11, 12). CIPO is also genetically heterogeneous, with most of the disease-causing genes (*FLNA*, *RAD21*, *SGOL1*, *ACTG2*, *MYH11*) involved in the development and function of the gut and bladder smooth muscles (13–19). In these myogenic cases, mixed alterations of intestinal smooth muscle (ISM) and enteric nervous system (ENS) are frequently described (13–17). To the best of our knowledge, a combination of HSCR and CIPO in the same patient has not been reported.

The ERBB family of receptor tyrosine kinases is comprised of 4 members, ERBB1–4, that are widely expressed in neuronal, epithelial, and mesenchymal cell types under physiological conditions (20, 21). The ERBB receptors play an essential role in the regulation of cell proliferation, survival, and differentiation, through activation of various signaling cascades including phosphatidylinositol 3-kinase (PI3K)/AKT and extracellular signal-regulated kinase (ERK) signaling (22, 23). Their main ligands are neuregulins; in particular, NRG1 (20, 24). Ligand-receptor binding triggers homo- or heterodimerization of ERBBs, cross-phosphorylation of the dimeric partners, and activation of downstream pathways (20, 21). Among the 4 members, ERBB3 has no intrinsic tyrosine kinase activity and its function is thus dependent on heterodimerization, preferably with ERBB2 (which by itself has a conformation preventing direct interaction with ligand) (25).

Somatic activating mutations in *ERBB2* and *ERBB3* have been reported in several solid cancers (26, 27), and a heterozygous germline activating variant of *ERBB3* in a myelodysplastic syndrome (erythroleukemia, OMIM 133180) (28). A homozygous splice site variant in *ERBB3* was reported in a consanguineous family with 29 affected individuals presenting congenital contracture syndrome type 2 with early lethality (LCCS2, OMIM 607598) (29–31). Recently, homozygous or compound heterozygous variants in *ERBB3* were also described in a case with LCCS, dysmorphic features, and knee and hip dislocations (32), and in a patient with a syndrome including intellectual disability, atrioventricular canal malformation, craniofacial anomalies, and immunodeficiency (33). To the best of our knowledge, no clearly pathogenic germline mutation of *ERBB2* has been reported in humans, but rare variants predicted to be damaging were found overrepresented in Chinese cases with short-segment HSCR (34). Also, in a single case, a combination of noncoding variants of unknown significance in *ERBB4* and *NRG1* has been observed (35). Finally, a genome-wide association study (GWAS) identified overrepresentation of 2 SNPs in intron 1 of *NRG1* in a Chinese cohort of patients with isolated HSCR (36), while mutational scans of the *NRG1* coding sequence identified rare missense variants of uncertain pathogenicity in a minority of isolated HSCR cases worldwide (37–39).

In mice, the knockout of either *Nrg1*, *Erbb2*, or *Erbb3* results in the absence or severe depletion of various neural crest–derived cells (40–44). Among these, absence of Schwann cells was reported in *Erbb2* and *Erbb*3 knockouts, and was proposed to cause the death of motor neurons in the ventral horn of the spinal cord and of sensory neurons in the dorsal root ganglia during development (42, 43). Recently, the ENS of neural crest–conditional *Erbb3* mutants (*Wnt1::Cre Erbb3*$^{lox/lox}$) was shown to be affected, with a reduction of 50% to 70% in the number of Phox2b-positive cells along the whole length of the gut. The same study also demonstrated a deficiency of esophageal ganglia and a reduction in the extent of the postgastric ENS in *Phox2b::Cre NRG1*$^{lox/lox}$ mutant mice, highlighting the role of NRG1/ERBB signaling in the migration of vagus nerve-associated neural crest cells to the gut (44).

Here, trio whole exome sequencing (WES) led to the identification of biallelic variants in *ERBB3* and *ERBB2* in 8 individuals with syndromic presentations at least in part implicating neural crest derivatives, from 5 families. Six patients had gut motility disorders, including HSCR, hypoganglionosis, and CIPO. In combination with thorough pathological, gene expression, and in vitro functional analyses that highlight a primary role of ERBB3 in enteric progenitors, this study underscores the role of NRG1/ERBB3/ERBB2 signaling in human gut development and indicates that disruption of this pathway results in a variable multisystemic syndrome, including complex gastrointestinal (GI) alterations.

Results

Clinical presentation and identification of ERBB3 and ERBB2 biallelic variations. With the aims of describing a syndrome combining HSCR and CIPO and identifying the disease-causing gene or genes, we studied a patient (F1:II-3) presenting with the combination of a complex neurocristopathy (short-segment HSCR, progressive axonal peripheral neuropathy, dysautonomia, and hypopigmentation), CIPO, hypoplasia of the olfactory bulbs, external auditory canal agenesis, and hearing loss (Figure 1A, Table 1, and Supplemental Table 1; supplemental material available online with this article; https://doi.org/10.1172/JCI145837DS1). His clinical manifestations did not correspond to a recognizable syndrome. Array-CGH (Agilent 60k) was normal. Trio WES led to the identification of compound heterozygous missense variants in the *ERBB3* gene (erb-b2 receptor tyrosine

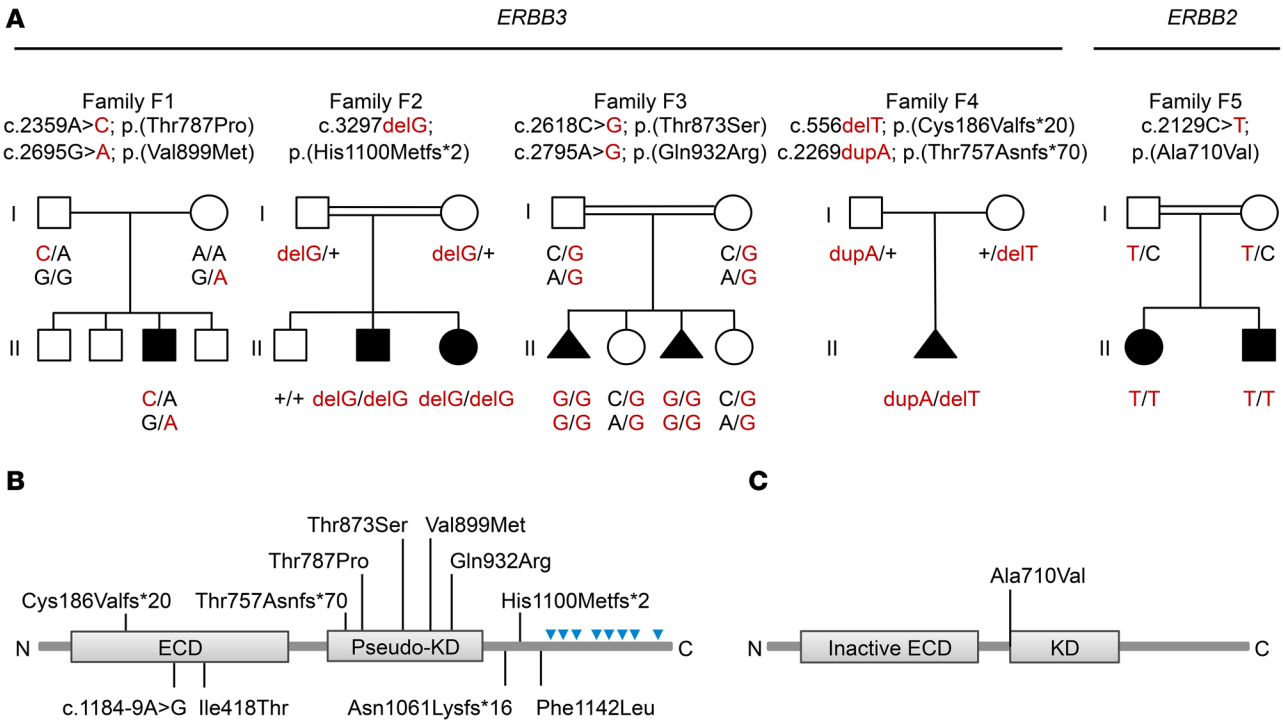

Figure 1. Biallelic *ERBB3* and *ERBB2* variations in 8 affected individuals from 5 families. (**A**) Pedigrees and segregation of *ERBB3* (NM_001982.3) and *ERBB2* (NM_004448.3) variants. Mutant alleles are indicated in red. (**B** and **C**) Schematic representation of ERBB3 (**B**) and ERBB2 (**C**) proteins showing the predicted consequences of variants identified in this study. *ERBB3* variants previously reported in developmental disorders are indicated below the schematic. The localization of putative phosphorylation sites are indicated by blue arrowheads. Inactive ECD: inactive extracellular domain; pseudo KD: pseudo kinase domain.

kinase 3; MIM: 190151, GenBank: NM_001982.3) in the affected individual (c.2359A>C, p.(Thr787Pro) and c.2695G>A, p.(Val899Met); Figure 1, A and B). Each variant was inherited from an unaffected parent, and was confirmed by Sanger sequencing (not shown) (Figure 1A, Family F1).

Through international collaborations, we subsequently recruited 4 unrelated families in which variants were identified in *ERBB3* or *ERBB2*, with affected individuals presenting multiple congenital anomalies, comprising both neural crest and extraneural crest features (Table 1, Supplemental Table 1, and Figure 1).

In the proband of family F2 (F2:II-2), a homozygous deletion of one nucleotide (c.3297delG, p.(His1100Metfs*2)) in *ERBB3* was identified by trio WES (Figure 1, A and B, Table 1, and Supplemental Table 1). Sanger sequencing confirmed the deletion and the expected segregation, with homozygosity in the proband and his affected sister (F2:II-3), and heterozygosity in both parents. The healthy sibling did not harbor the variant (Figure 1A). The proband, a male, combines HSCR and other manifestations including ptosis, external ear agenesis, and hearing loss. His affected sister presented similar clinical manifestations plus olfactory bulb agenesis (Table 1 and Supplemental Table 1).

In family F3, WES analysis of 2 affected fetuses, F3:II-1 (aborted at 16 weeks of gestation [WG]) and F3:II-3 (deceased at 15 WG), identified homozygosity for 2 variants in *ERBB3* (c.2618C>G, p.(Thr873Ser) and c.2795A>G, p.(Gln932Arg)). Their parents and 2 healthy siblings are heterozygous for both variants (i.e., the 2 variants are on the same allele) (Figure 1A, Family F3, and Figure 1B). In family F4, trio WES identified compound heterozygosity for 2 frameshift variants (c.556delT, p.(Cys186Valfs*20) and c.2269dupA, p.(Thr757Asnfs*70)) in a fetus aborted at 18 WG (F4:II-1), with each variant inherited from one parent (Figure 1A and Figure 1B). All 3 affected fetuses of families F3 and F4 presented intrauterine growth retardation, akinesia, arthrogryposis with multiple pterygiums, with or without cardiac malformations, while macroscopic examination of the intestine showed no dilatation, atresia, or volvulus (Table 1 and Supplemental Table 1).

In family F5, WES analysis of F5:II-1 identified a homozygous missense variant (c.2129C>T, p.(Ala710Val)) within *ERBB2* (MIM : 164870, GenBank: NM_004448.3). Sanger sequencing confirmed that the 2 affected children are homozygous while the healthy parents are heterozygous for the *ERBB2* variant (Figure 1, A and C). The proband, a female, born to consanguineous parents, presented severe constipation that eased after 5 years of age, axonal peripheral neuropathy, ptosis, perceptive hearing loss, and clubfeet (Table 1 and Supplemental Table 1). Her brother had a similar clinical presentation, with short-segment HSCR.

Histologic characterization of gastrointestinal and muscle alterations. In patient F1:II-3 with both HSCR and CIPO, histology of the rectum showed thick extrinsic nerve fibers and the absence of ganglion cells (Figure 2A). Various abnormalities in the ganglionic segments were also noticed, including atrophy of the longitudinal outer muscular layer in the colon and ectopic location of the myenteric plexuses within the outer muscular layer in the small intestine (Figure 2A). Immunohistochemistry with S100 (a marker of glial cells) confirmed the ectopic localization of enteric ganglia

Table 1. *ERBB3* and *ERBB2* variations and associated phenotypes

Causal gene	*ERBB3* (NM_001982.3)						*ERBB2* (NM_004448.3)	
Affected individuals	F1:II-3	F2:II-2	F2:II-3	F3:II-1	F3:II-3	F4:II-1	F5:II-1	F5:II-2
HSCR	+	+	+	+	NA	+	NA	+
Hypoganglionosis	–	+	+	–	NA	–	NA	+
Intestinal smooth muscle abnormalities	+	–	–	–	NA	–	NA	NA
CIPO	+	–	–	NR	NR	NR	–	–
Arthrogryposis	–	–	–	+	+	+	+	+
Peripheral neuropathy	+	–	–	NR	NR	NR	+	+
Olfactory bulb agenesis	+	–	+	NA	NA	+	NA	NA
External auditory canal agenesis	+	+	+	+	+	+	–	–
Hearing loss	+	+	+	NR	NR	NR	+	+
Ptosis	–	+	+	NR	NR	NR	+	+
Dysautonomia	+	–	–	NR	NR	NR	–	–
Pigmentation defect	+	–	–	–	–	–	–	–
Cardiac defect	–	–	–	+	+	–	–	–
cDNA	c.2359A>C c.2695G>A	c.3297delG	c.3297delG	c.2618C>G c.2795A>G	c.2618C>G c.2795A>G	c.556delT c.2269dupA	c.2129C>T	c.2129C>T
Protein	p.(Thr787Pro) p.(Val899Met)	p.(His1100Metfs*2)	p.(His1100Metfs*2)	p.(Thr873Ser) p.(Gln932Arg)	p.(Thr873Ser) p.(Gln932Arg)	p.(Cys186Valfs*20) p.(Thr757Asnfs*70)	p.(Ala710Val)	p.(Ala710Val)
Inheritance	Comp. Het.	Hom.	Hom.	Hom.	Hom.	Comp. Het.	Hom.	Hom.
GnomAD	0 0	0	0	0 0	0 0	1/251484/0 0	0	0
SIFT	0 0	NA	NA	0 0	0 0	NA NA	0.04	0.04
Polyphen2	1 1	NA	NA	1 1	1 1	NA NA	1	1
CADD	27 31	NA	NA	31 28.3	31 28.3	NA NA	28	28

Variant frequency is presented as allele count/allele number/number of Hom. or 0 if absent from the GnomAD database; variant pathogenicity is predicted by SIFT (close to 0), Polyphen2 (close to 1), and CADD scores. HSCR, Hirschsprung disease; CIPO, chronic intestinal pseudo-obstruction; NR, not relevant; Comp. Het., compound heterozygous; Hom., homozygous.

in the small intestine (Figure 2B). We also examined markers of smooth muscle, smooth muscle actin (SMA), and desmin. As previously observed in most patients with CIPO and some controls (45), an absence of SMA was observed in the circular inner muscular layer of the small intestine, while the desmin distribution appeared normal (Figure 2B). Staining for cKIT, a marker of interstitial cells of Cajal (ICCs), showed normal distribution of these cells (Figure 2B).

In both HSCR cases of family F2, histology revealed a very short (< 2 cm) distal aganglionic segment without overt extrinsic nerve fibers, and a long transition zone with rare scattered ganglion cells (Figure 2, C and D), arguing for a histological diagnosis of hypoganglionosis (46).

In patient F5:II-2, histology revealed a lack of ganglion cells and a hyperplasia of nerve fibers in the colon resection specimen (Figure 2E).

Following these observations, a retrospective investigation of the digestive tracts of the 2 fetuses F3:II-1 (Figure 3A) and F4:II-1 (Figure 3B) was performed. Total colonic aganglionosis extending to the stomach in F3:II-1 and to the small intestine in F4:II-1 was observed in H&E-stained sections, and confirmed by the absence of PHOX2B and S100 staining (Figure 3, A and B). SMA staining was comparable to that of an age-matched control in each case (Figure 3, A and B).

Besides the ENS defects, histology of muscle tissues of the affected fetuses of families F3 and F4 provided evidence of skeletal myopathy (Figure 4). Indeed, a high proportion of myotubes with a centered nucleus were observed in 2 fetuses F3:II-1 (Figure 4A) and F3:II-3 (Figure 4B), while in the age-match controls, most muscle fibers are mature with nuclei positioned at the periphery (Figure 4, A and B). In the fetus F4:II-1, myotubes with centralized nuclei were also found but to a lesser extent (Figure 4C), and staining of slow and fast myosin heavy chains showed a physiological presence of type I and type II muscle fibers (Figure 4E). Analysis at ultrastructural level by electron microscopy showed isolated primary myotubes in fetus F4:II-1, while in the control, secondary myotubes were observed apposed to the primary myotubes (Figure 4D). Histology of cervical spinal cord of fetus F4:II-1 displayed normal morphology and density of both motoneurons in the anterior horn and sensory neurons in the dorsal root ganglia (Figure 4, F and G).

Investigation of the cell type specificity of ERBB3/ERBB2 function in ENS and ISM development. ERBB3 expression was previously reported in the enteric plexuses and possibly in the ISM in mouse

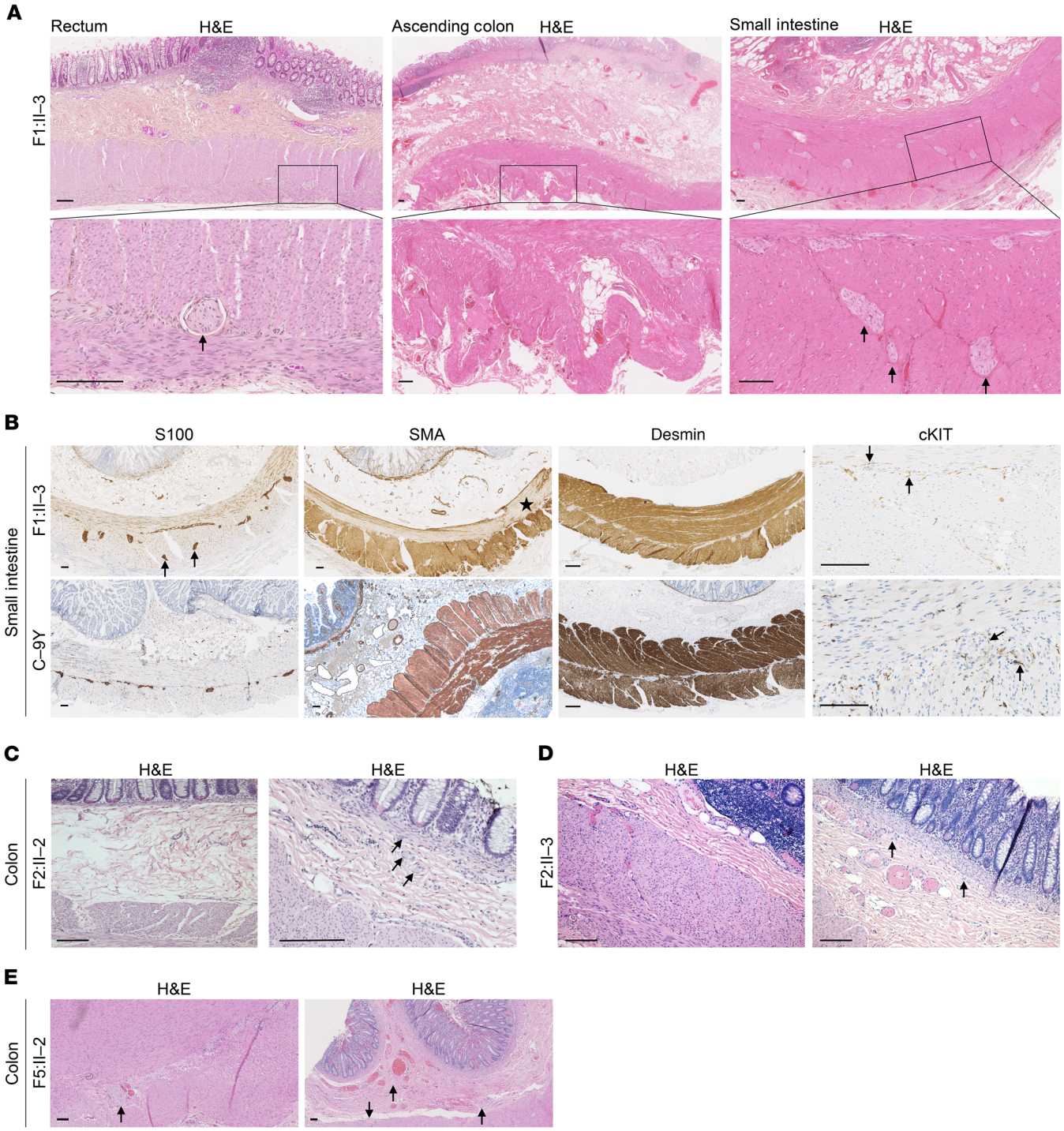

Figure 2. Histology of gut specimens from patients with *ERBB3* or *ERBB2* mutations. (**A** and **B**) Patient F1:II-3. (**A**) H&E-stained sections showed aganglionosis and hypertrophic nerve fibers (arrow) in the rectum, atrophy/disorganization of the external muscularis in the colon, and ectopic location of myenteric plexuses (arrows) within the external muscularis of the small intestine. (**B**) Immunohistochemistry for S100 indicated presence of enteric glia and ectopic localization of enteric plexuses (arrows). Lack of SMA staining in the internal muscularis (star) of the small intestine, and normal desmin staining were observed. cKIT staining appeared normal (arrows point to ICCs). (**C**) Patient F2:II-2 and (**D**) Patient F2:II-3. H&E-stained sections revealed a short distal agangliononic segment without overt hyperplastic nerves (photos on the left-hand side), followed by a long hypoganglionic segment containing rare scattered ganglion cells (arrows in photos on the right-hand side). (**E**) Patient F5:II-2. H&E-stained sections showed a lack of myenteric and submucosal ganglion cells and a hyperplasia of nerve fibers in the colon (arrows). Scale bars: 100 μm.

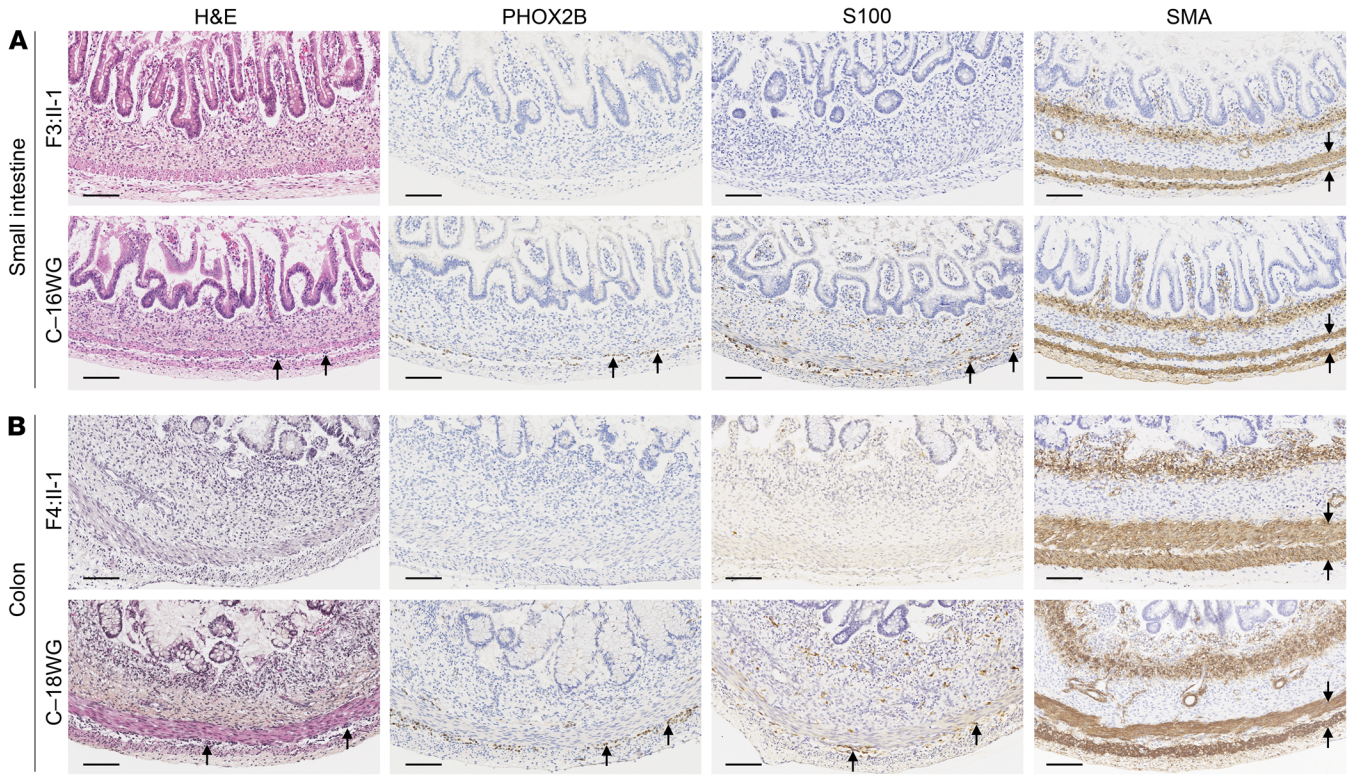

Figure 3. Histology of gut specimens from fetuses with *ERBB3* mutations. (**A**) Fetus F3:II-1 and (**B**) fetus F4:II-1, along with age-matched controls (C-16WG and C-18WG, respectively). H&E-stained sections showed total colonic aganglionosis, confirmed by absence of PHOX2B and S100 staining in both fetuses. In the controls, enteric neurons and glia were observed (arrows). SMA staining was normal (arrows). Scale bars: 100 μm.

and/or human (47, 48). However, scrutinizing human scRNA-seq data sets revealed no/low detectable expression of *ERBB3* and *ERBB2* in the intestinal muscle cell population identified by expression of *ACTA2* (encoding smooth muscle-2 actin) (49). In mouse, ENS scRNA-seq data sets generated at E15.5 and E18.5 further ascertained that *ErbB3* and *ErbB2* are expressed almost exclusively in the enteric progenitors and glial populations (Figure 5A). No/lower expression was found in neurons (Figure 5A). Altogether, these data suggest that the impact of *ERBB3* and *ERBB2* variants might be cell autonomous in the ENS and non–cell autonomous in the ISM.

To determine whether NRG1/ERBB3 signaling from the neural crest–derived ENS can impact ISM development, we evaluated gut muscle development in neural crest–specific *ErbB3*-deficient mice. Histological analysis and immunohistochemistry using TUJ1 (a neuronal marker) and SMA confirmed hypoganglionosis as previously described (44), but we observed no gross alteration of the 2 muscle layers in mutants compared with controls at E17.5, the latest stage that mutants could be analyzed before embryonic death at day E18. Specific invalidation of *Erbb3* in neural crest cells thus does not impact the ISM, at least before birth (Figure 5B).

Reduced expression and impaired function of mutant ERBB3 and ERBB2. Out of the 7 *ERBB3* variants identified, 3 were frameshifts that were either absent or present at very low frequency in the gnomAD database and with no homozygosity reported (Table 1). The c.3297delG variant of F2:II-2 and F2:II-3 is located in the penultimate exon of *ERBB3,* whereas c.556delT and c.2269dupA of F4:II-1 are located in exons 5 and 19, respectively. They are predicted to lead to premature stop codons 2, 20, and 70 amino acids downstream and, if translated, would lead to truncated proteins, lacking essential functional domains or the C-terminal tail rich in phosphorylation sites (Figure 1B) (50). Alternatively, the mutant mRNAs could be degraded by nonsense-mediated mRNA decay (NMD). RT-qPCR experiments performed on fibroblasts confirmed that the *ERBB3* mRNA was significantly lower in cells from F2:II-2, compared with his mother (F2:I-2) and a control (Figure 6A). cDNA sequencing confirmed the presence of the variant in the quantified transcripts (Figure 6B). Samples from family F4 were not available for testing.

The 5 missense variants (4 in *ERBB3* and 1 in *ERBB2*) were also absent in the gnomAD database and predicted to be damaging by SIFT, Polyphen-2, and CADD scores (Table 1). The affected amino acids are highly conserved and located in the pseudo-kinase domain of ERBB3 or the kinase domain of ERBB2 (Figure 1, B and C, and Figure 7, A and B). 3D modeling using the crystal structure of these domains predicted no modification due to the ERBB2 variant, but modifications of hydrogen bonds were predicted for p.(Thr787Pro), (Thr873Ser), and p.(Gln932Arg) substitutions in ERBB3 (Figure 7, C and D). These changes may destabilize the protein and/or modify its conformation and thus, affect its function.

The impact of each variant on ERBB3 and ERBB2 subcellular localization and function was further analyzed in vitro. Transfec-

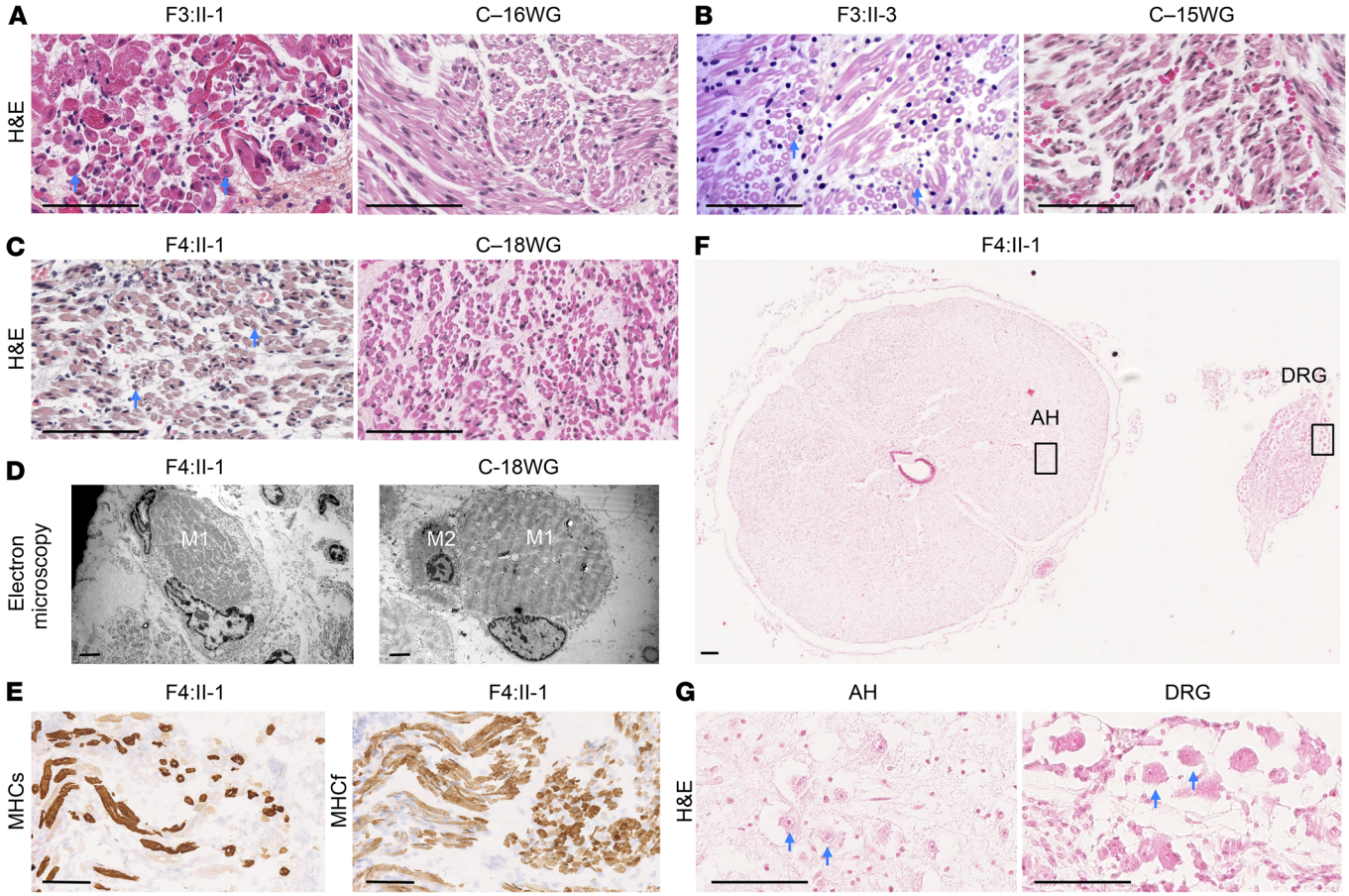

Figure 4. Histology of skeletal muscles, the anterior horn of the spinal cord and dorsal root ganglia of fetuses with *ERBB3* mutations. (**A**–**C**) H&E-stained sections of muscle specimens from F3:II-1 (**A**, quadriceps femoris muscle at 16 WG), F3:II-3 (**B**, deltoid muscle at 15 WG), and F4:II-1 (**C**, psoas muscle at 18 WG). Note the presence of the unequal caliber of muscle fibers with the presence of numerous myotubes characterized by central nuclei (blue arrows) compared with the control muscles (C-16WG, C-15WG, and C-18WG psoas muscles), where muscle fibers are homogeneous in size and density with most nuclei positioned at the periphery of mature fibers. (**D**) Analysis at the ultrastructural level by electron microscopy shows isolated primary myotubes (M1) in fetus F4:II-1, while in the control, secondary myotubes (M2) were observed apposed to the primary myotube (M1). (**E**) Immunohistochemical analyses using NCL-MHCs and NCL-MHCf antibodies (staining slow and fast myosin heavy chains, respectively) showed the presence of type I and II myotubes, respectively. (**F**) Preserved cyto-architecture of cervical spinal cord of fetus F4:II-1. AH: anterior horn; DRG: dorsal root ganglion. (**G**) Higher magnification of boxed regions in **F**. At the cellular level, both motoneurons in the anterior horn (blue arrows in AH) and sensory neurons in the dorsal root ganglia (blue arrows in DRG) displayed normal morphology and density. Scale bars: 100 μm in **A**–**C**, **E**–**G**; 2 μm in **D**.

tion of expression vectors containing WT or mutated tagged versions of human ERBB3 and ERBB2 cDNA followed by immunocytofluorescence experiments using antibodies directed against each tag and phalloidin (a marker of actin, for visualization of cell shapes), revealed that none of the variants affects the localization of the resulting proteins at the cell membrane (Figure 8A).

Next, we cotransfected Neuro-2a cells with expression vectors containing WT ERBB2 and WT or mutated forms of ERBB3 cDNA, treated the cells with or without NRG1, and analyzed ERBB3 phosphorylation levels by Western blotting. An almost total absence of ERBB3 phosphorylation was observed upon analysis of the 2 variants identified in family F1, p.(Thr787Pro) and p.(Val899Met), with or without NRG1. The p.(Thr873Ser) and p.(Gln932Arg) behaved as WT in this assay (Figure 8, B and C, for quantification). The phosphorylation of ERBB2 was also impaired for p.(Thr787Pro) and p.(Val899Met), and no significant increase in ERBB2 phosphorylation level was observed upon NRG1 treatment for all 4 mutants, suggesting alteration of downstream signaling (Figure 8B and quantification in Figure 8D). Similarly, Western blot analysis revealed a drastic decrease of both ERBB2 and ERBB3 phosphorylation upon analysis of the *ERBB2* variant (Figure 8E and quantifications in Figure 8, F and G). Altogether, these functional analyses demonstrate either total or partial loss-of-function consequences for all missense variants.

Discussion

Here we report 8 patients carrying homozygous or compound heterozygous variants in *ERBB3* or *ERBB2* and presenting with a broad spectrum of developmental anomalies associating neural crest and extra-neural crest features, including intestinal dysmotility. In vitro studies showed that these variants were either loss-of-function mutations or hypomorphic alleles due to decreased expression or altered phosphorylation of the receptors. *ERBB3,* and also *ERBB2,* are thus further examples of genes in which loss-

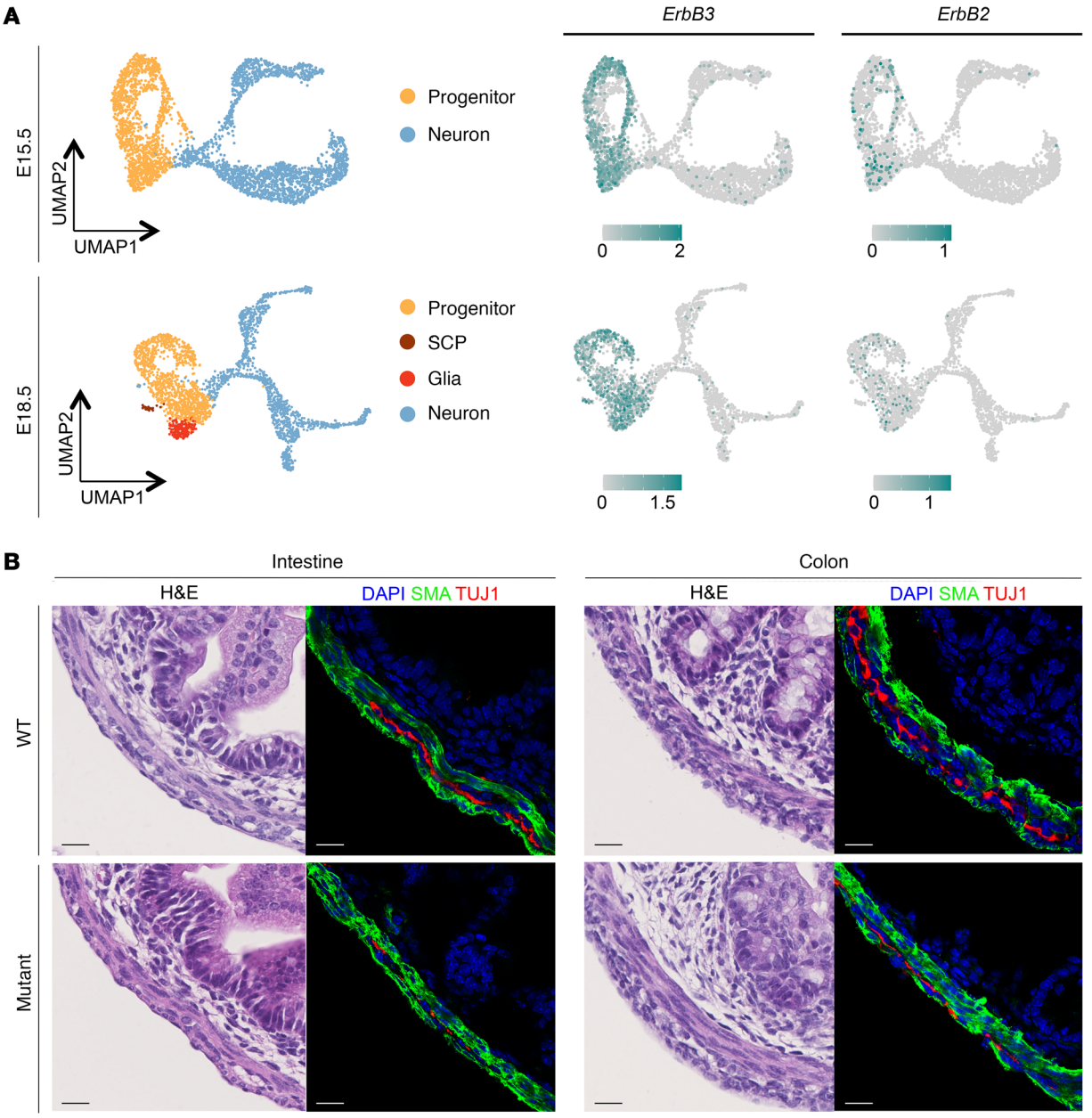

Figure 5. Investigation of the cell type specificity of ERBB3/ERBB2 in ENS and ISM development. (**A**) Expression of *ErbB3* and *ErbB2* in different populations identified by scRNA-seq at E15.5 and E18.5. Uniform Manifold Approximation and Projection (UMAP) representations indicate clusters corresponding to progenitors, Schwann cells precursors (SCP), enteric glia, and neurons. Feature plots show expression of *ErbB3* and *ErbB2*. Color bars indicate expression level with maximum cut off at the 90th percentile. (**B**) H&E staining and immunohistochemistry for SMA (green) and TUJ1 (red) on small intestine and colon sections from WT and *Wnt1::Cre Erbb3*$^{lox/lox}$ (Mutant) embryos at E17.5 show normal ISM layer organization. In each case, 10 to 20 sections of $n = 3$ controls and $n = 3$ mutants were analyzed. Scale bars: 20 μm.

of-function and activating mutations are reported in developmental disorders and cancer, respectively.

In the literature, intestinal defects were not documented in patients with biallelic *ERBB3* variants (29–33). In our study however, 4 patients (F1:II-3, F2:II-2, F2:II-3, and F5:II-2) presented severe intestinal dysmotility due to HSCR, hypoganglionosis, and/or CIPO. Following identification of *ERBB3* variants, retrospective examination of gut histology revealed total colonic aganglionosis in both fetuses for which samples were available (F3:II-1 and F4:II-1). Altogether, GI alterations were found in at least 6 of 8 cases, making them the most common feature of the *ERBB3/ERBB2*-associated phenotype in our series. In particular, the combination of HSCR and CIPO in patient F1:II-3 is a previously unreported finding, to the best of our knowledge. Gut histology further revealed that ganglionic regions of patients with ERBB3/ERBB2 loss of function can be abnormal, causing complex gut dysmotility that should be anticipated. For better patient care and counseling, we also propose that patients presenting syndromic HSCR with persistent postoperative gut motility disorders should be screened for *ERBB3/ERBB2* genetic variations.

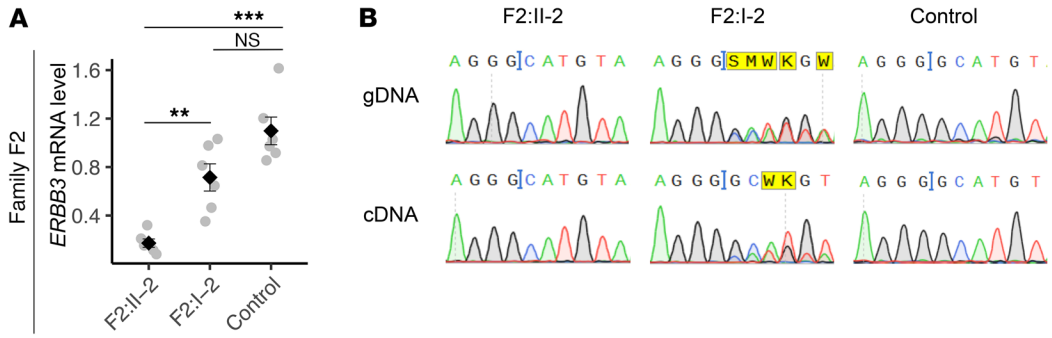

Figure 6. Decreased *ERBB3* expression due to the c.3297delG variant. (**A**) *ERBB3* mRNA expression level in fibroblasts determined by RT-qPCR. F2:II-2 and F2:I-2 represent the patient and his mother, respectively. The relative abundance of the *ERBB3* amplicon was normalized to the *GUSB* internal control and presented relative to that of cells from the control. Data represent mean ± SEM (in black) of relative gene expression of $n = 6$ independent biological replicate experiments (in gray) performed in triplicate. Statistical differences were determined using a 2-tailed t test on ΔCt values and Holm-Bonferroni correction. NS: $P > 0.05$. $^{**}P < 0.01$, $^{***}P < 0.001$. (**B**) Sanger sequencing identified the c.3297delG variant in genomic DNA (gDNA) extracted from peripheral blood samples and in cDNA amplified from the patient and his mother's fibroblast, and its absence in a control.

As for all monogenic syndromes predisposing to HSCR described thus far, the HSCR trait shows high but incomplete penetrance in the *ERBB3/ERBB2*-associated multisystemic syndrome. While the *ERBB3* variants identified in our cohort appear sufficient to cause HSCR, we cannot exclude the possibility that additional genetic factors may contribute to the phenotype in the affected siblings reported here with a homozygous *ERBB2* variant. Investigation of a larger cohort of *ERBB3/ERBB2*-variant carriers with or without HSCR would allow us to address this issue. Regarding the ligand, the association of *NRG1* rare variants and a *RET* intronic low-predisposition variant has previously been reported in less than 1% of isolated HSCR cases in Spanish and Chinese populations (37–39). Our own screen of 121 French individuals with HSCR revealed a de novo truncating variant in *NRG1* (NM_013960.4: c.608C>G, p.(Ser203*)) in a male patient with isolated short-segment HSCR, who also harbored a low-effect noncoding variant in *RET* (our unpublished observations). Altogether, these data demonstrate that dysregulation of the NRG1/ERBB3/ERBB2 pathway can lead to HSCR in humans, and that the penetrance of this trait may be influenced by variations in the *RET* locus.

Apart from the combination of HSCR and CIPO in the patient F1:II-3, the observed GI manifestations of the patients studied here are reminiscent of those described in patients with *SOX10* monoallelic variants. Initially implicated in type IV Waardenburg syndrome (WS4, defined by pigmentation defects, deafness, and HSCR), *SOX10* variants have now been identified in patients with either HSCR, hypoganglionosis, or CIPO (51–55). In the 4 reported CIPO cases, rectal and intestinal biopsies showed normal ganglionic cells, but the muscle layers were not scrutinized (53–55). Considering the role of SOX10 in ENS development, CIPO is probably neurogenic in these cases. In our study, one of the patients with HSCR presented quantitative and topologic anomalies of the ENS and abnormal ISM upon histology of intestinal specimens. Whether these alterations are independent or interdependent is unclear. In favor of the latter hypothesis, it has been shown that ENS defects may impact gut muscle cell differentiation and vice versa (56, 57). Indeed, the ablation of neural crest–derived cells in the stomach of chick embryos causes a reduction in the expression of smooth muscle differentiation markers (56). The inhibition of early ISM differentiation also hinders the patterning of the enteric plexus in chick (57). However, mesenchymal differentiation initiates well before colonization by enteric progenitors in the colon (58), and the ISM is able to form ex vivo despite the absence of enteric plexuses (57). Of interest, analysis of scRNA-seq data showed prominent *ErbB3* expression in the murine ENS, while no detectable *ERBB3* expression was observed in ISM in human embryos (49). Our reevaluation of the phenotype of neural crest–specific *Erbb3*-deficient mice also showed no gross alteration of the 2 muscle layers in mutants compared with controls at E17.5, suggesting that the ISM develops independently of the ENS-derived ERBB3 signaling up to this stage. Altogether, these data suggest that the CIPO identified in patient F1:II-3 is likely neurogenic, while the cause of the ISM abnormality is unclear. Interestingly, most CIPO cases are classified as myogenic, with mixed alterations of ENS and ISM observed, highlighting the difficulty in attributing a primary cause for this disorder.

In addition to gut alterations, a peripheral neuropathy was described in 3 of 8 patients reported here. F1:II-3 suffered from progressive peripheral neuropathy and dysautonomia with tachycardia, hyperesthesia, and hyperhidrosis. In this patient, quantitative sudomotor function testing measured by electrochemical skin conductance provided evidence for the degeneration of the unmyelinated nerve fibers innervating sweat glands (59). Consecutive electroneuromyography studies displayed a progressive axonal motor and sensory neuropathy with decreased nerve conduction amplitude, while nerve conduction velocities were in the normal range. Of interest, knockout of either *Erbb3* or *Erbb2* in mice results in degeneration of motor neurons in the ventral horn and sensory neurons in the dorsal root ganglia (42, 43). However, these neuronal defects were considered as non–cell autonomous and secondary to a depletion or total absence of Schwann cell precursors along peripheral nerves (42, 43). The differences observed between mice and patient F1:II-3 have no explanation so far and require further investigation.

Besides a complex neurocristopathy, extra-neural crest anomalies were noted in the patients reported here and in others

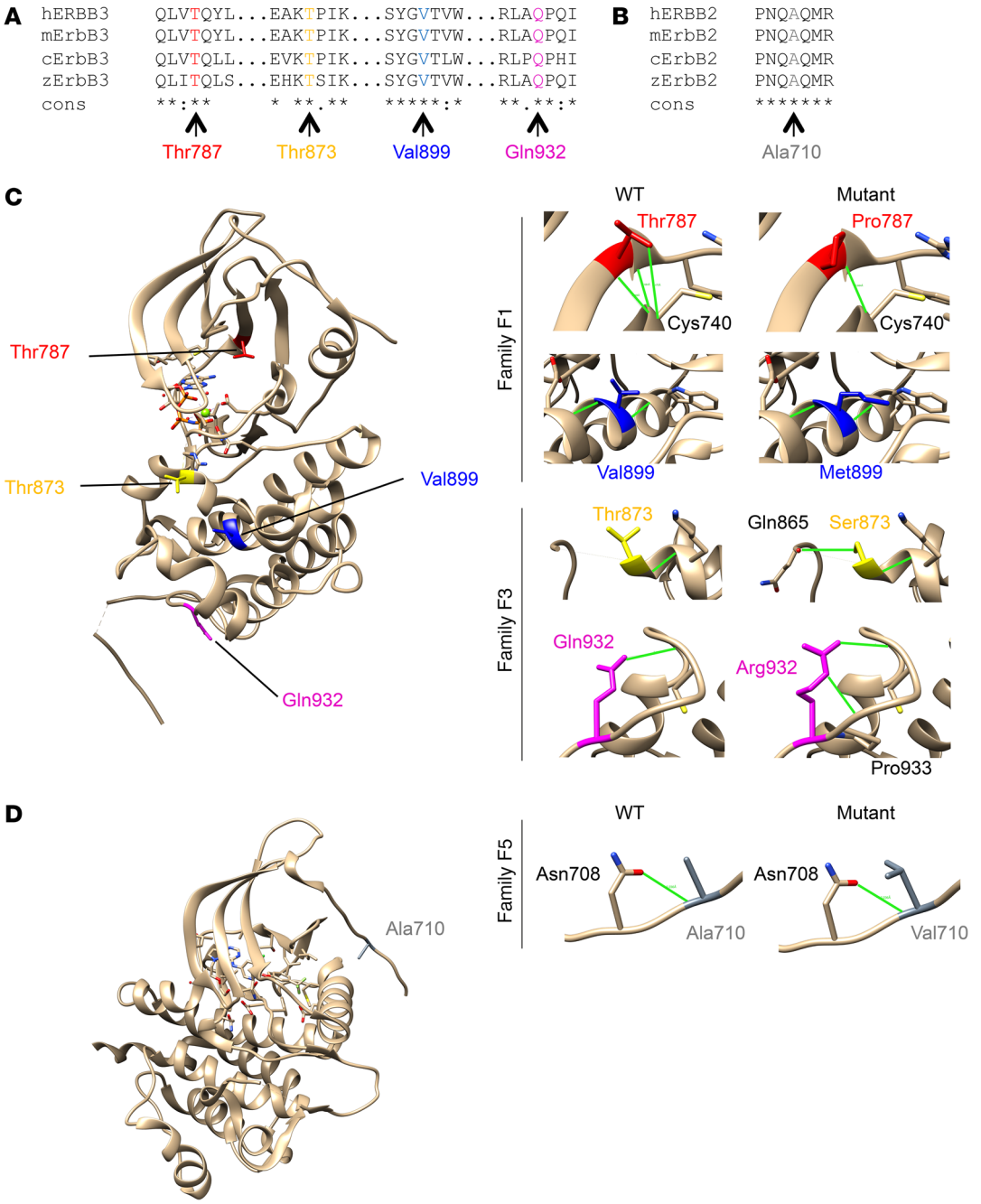

Figure 7. Conservation and 3D analysis of ERBB3 and ERBB2 variants. (**A** and **B**) Conservation of the relevant amino acids in human (h), mouse (m), chick (c), and zebrafish (z); asterisks indicate conserved residues in ERBB3 (**A**) and ERBB2 (**B**). (**C**) 3D modeling showing the positions of the identified variants on the crystal structure of the pseudo-kinase domain of ERBB3 (left side) and structural analysis of WT and mutants (right side). Hydrogen bonds are shown in green. Mutations are indicated in different colors (red: p.(Thr787Pro); blue: p.(Val899Met); yellow: p.(Thr873Ser); pink: p.(Gln932Arg)) and presented by family. The WT proteins are depicted in the left column and the mutant versions on the right. Note the p.(Thr787Pro) variant is expected to cause a loss of 2 hydrogen bonds between the Thr787 and the Cys740 residues, while p.(Thr873Ser) and p.(Gln932Arg) are predicted to add a hydrogen bond between the substituted amino acids and the Gln865 or the Pro933 residues, respectively. (**D**) 3D modeling showing the position of the identified variant on the crystal structure of the kinase domain of ERBB2 (left side) and structural analysis of WT and mutant (gray: p.(Ala710Val); right side). Note absence of modifications.

in the literature with biallelic variants in *ERBB3*. Arthrogryposis was previously attributed to atrophy of neurons in the anterior horn following autopsy of one individual (29). However, the fetus F4:II-1 in our cohort had normal motor and sensory neurons, while altered skeletal muscle cells were documented in all 3 fetuses: F3:II-1, F3:II-3, and F4:II-1. Indeed, histological findings of muscle fibers with centralized nuclei suggest either a pathological development or a maturation delay of skeletal muscles (60, 61). In favor of the latter, isolated primary myotubes and a paucity of secondary myotubes were observed in the fetus F4:II-1, while type I and type II fibers appeared normal. These observations argue for myogenic arthrogryposis in the affected fetuses, which

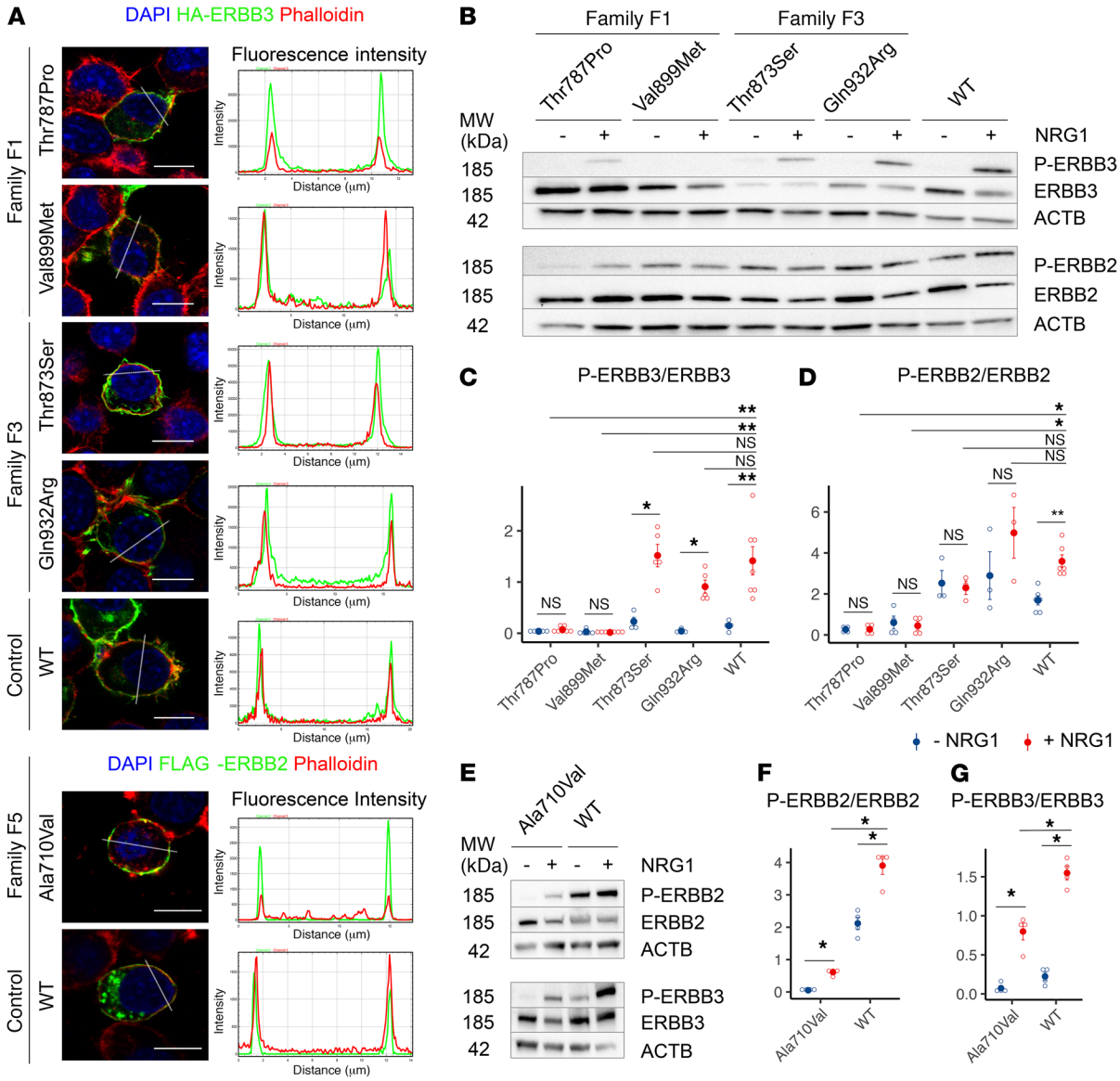

Figure 8. Functional consequences of *ERBB3* and *ERBB2* missense variants. (**A**) Subcellular localization of ERBB3 and ERBB2 mutant proteins. DAPI (blue), an antibody directed against the tagged ERBB3 (anti-HA, green) or tagged ERBB2 (anti-FLAG, green) receptors and phalloidin (red) were used to visualize subcellular localization of mutant proteins. In each case, 100 cells in each of $n = 3$ independent experiments were observed. Merge representative images are presented, with fluorescence intensity graphs on the right depicting the colocalization, with red and green lines indicating the corresponding fluorescence of phalloidin and tagged protein, respectively. Variants are presented per family and compared with controls (WT ERBB3 or WT ERBB2). Scale bars: 10 μm. (**B**–**G**) Phosphorylation of ERBB3 and ERBB2 analyzed by Western blot, following transfection of Neuro-2a cells with WT or mutant ERBB3- and ERBB2-encoding plasmids. Representative gels (**B** and **E**) along with quantifications (**C**, **D**, **F**, and **G**, respectively) are shown. Actin beta (ACTB) was used as loading control. Cells were untreated (–) or treated (+) with NRG1. ERBB3 mutants are shown in **B**–**D** and the ERBB2 mutant in **E**–**G** compared with WT proteins (WT). In **C**, **D**, **F**, and **G**, data represent mean ± SEM. Statistical differences were determined from data of at least $n = 3$ independent biological replicate experiments using Mann-Whitney tests. After Holm-Bonferroni correction, NS: $P > 0.05$, $^*P < 0.05$, $^{**}P < 0.01$. MW: molecular weight.

is in accordance with the involvement of ERBB3 in the development of skeletal muscles (62, 63). Other nonneural crest defects are hypoplasia or agenesis of the olfactory bulbs in 3 affected individuals (F1:II-3, F2:II-3 and F4:II-1), in line with the expression of *ERBB3* in the olfactory bulbs and olfactory epithelium (24). Finally, mixed alterations of neural crest and nonneural crest derivatives might explain the tetralogy of Fallot in the fetus F3:II-3, as well as microretrognathia and the anomalies of the auricles and the external ear canal observed in all affected individuals with biallelic variants in *ERBB3* in our cohort.

Altogether, we have delineated a broad spectrum of developmental anomalies involving neural crest– and nonneural crest–derived tissues, due to dysregulation of the NRG1/ERBB3/ERBB2 pathway. The GI dysmotility observed in affected individuals is complex and can manifest as HSCR, hypoganglionosis, and/or CIPO in various combinations.

Methods

Patients, exome sequencing, and variant prioritization. In this study, we included 8 affected individuals presenting complex neurocristopathies

and/or extra-neural crest features: 5 patients with neurocristopathies (4 of them with HSCR, 3 with peripheral neuropathy) and 3 fetuses with arthrogryposis multiplex congenita. The major clinical features of each case are summarized in Table 1 and details are provided in Supplemental Table 1 and in the Supplemental Data. WES and data analysis were performed as previously described (64) using genomic DNA isolated from blood leukocytes or fetal lung. Upon exome analysis, no mutations in genes previously associated with HSCR or other ENS disease were found (3).

Histology and immunohistochemistry on tissues from patients and controls. Histological samples were formalin-fixed and paraffin-embedded. Four-μm-thick sections were stained with H&E. Immunohistochemical studies were performed on formalin-fixed, paraffin-embedded tissue sections on a Leica Bond 3 Max system, using the following antibodies: anti-S100 (Dako, Z0311, RRID:AB_10013383, 1/1000), anti-SMA (Dako, 1A4, RRID:AB_2223500, 1/300), anti-Desmin (Agilent, M0760, RRID: AB2335684, 1/100), c-KIT (CD117, Agilent, A4502, 1/100), anti-PHOX2B (Abcam, ab183741, RRID:AB_2857845, 1/1000), anti-Myosin heavy chain (slow) (NCL-MHCs, Visionbiosystem Novocastra, 1/60, clone WB-MHCs), and anti-Myosin heavy chain (fast) (NCL-MHCf, Visionbiosystem Novocastra, 1/30, clone WB-MHCf). All slides were scanned and visualized using NDPview2 software. Muscle biopsies were fixed in glutaraldehyde and embedded in Epon for electron microscopy examination.

Histology and immunohistochemistry on tissues from ErbB3-deficient mice. *Erbb3*$^{lox/lox}$ animals (Erbb3tm3Cbm/Erbb3tm3Cbm, RRID: MGI:5588162, maintained on B6D2F1background, a gift from C. Birchmeier, Max Delbrück Center for Molecular Medicine, Berlin, Germany) were crossed with the *Wnt1::Cre* line (129S4.Cg-E2f1Tg(Wnt1-cre)2Sor/J, RRID: IMSR_JAX:022137). Litters were then intercrossed to obtain E17.5 embryos of interest. Primers used for genotyping are provided in Supplemental Table 2. Mouse guts were dissected and fixed in 4% paraformaldehyde, embedded in paraffin, sectioned, and stained with H&E. Alternatively, fixed tissues were frozen in Optimal Cutting Temperature media (OCT, Sakura), cut into 8 μm sections and used for immunohistochemistry experiments using the following antibodies: anti-SMA (Abcam, ab5694, rabbit, 1/300), anti-TUJ1 (Covance, MMS-435P, mouse, 1/1000), anti-rabbit Alexa Fluor 488 (Invitrogen, 1/500), and anti-mouse Cy3 (Invitrogen, 1/500). Preparations were then mounted in Vectashield containing DAPI medium (Vector Laboratories) and observed using a Zeiss Confocal LSM 700.

RNA isolation and RT-qPCR. Fibroblasts were isolated from skin biopsies from patient F2:II-2 and his mother F2:I-2 and grown in reduced serum medium (Opti-MEM, Life Technologies) supplemented with 10% FBS, 100 μg/mL streptomycin, and 100 U/mL penicillin (Life Technologies) at 37°C, 5% CO_2. Along with an appropriate control, these fibroblasts were used to extract total RNA using the RNeasy Mini Kit, and treated with DNase from an RNase-free DNase Set (Qiagen). cDNA was reverse transcribed from 500 ng total RNA using the Verso cDNA Synthesis Kit (Thermo Scientific). ERBB3 cDNA levels were then measured by quantitative PCR using the GoTaq qPCR Master Mix (Promega) on a Mastercycler RealPlex^2 (Eppendorf) using the primers listed in Supplemental Data.

Modeling of the human ERBB2 and ERBB3 variants. Structural analysis was performed on crystal structures of the pseudo-kinase domain of ERBB3 (PDB ID: 3KEX) (65) and the kinase domain of ERBB2 (PDB ID: 3PP0) (66) using the UCSF Chimera software (https://www.cgl.ucsf.edu/chimera/). The hydrogen bonds between the WT or mutated residues and the surrounding amino acids were visualized for comparison.

Plasmids and site-directed mutagenesis. The full-length human ERBB3 (NM_001982.3) and ERBB2 (NM_001005862.2) cDNA with hemagglutinin peptide (HA) tags cloned into the pcDNA3.1 vector (pcDNA3.1-HA-ERBB3 and pcDNA3.1-HA-ERBB2) were a gift from Bridget Wilson's lab at the University of New Mexico (67). The HA tag in the pcDNA3.1-HA-ERBB2 construct was subsequently replaced by the FLAG tag using an In-Fusion HD Cloning Kit following the manufacturer's instructions (Takarabio). Site-directed mutagenesis was performed to introduce specific single-nucleotide variations into the ERBB3 and ERBB2 cDNA in the above plasmids using mutation-containing primers and the Phusion Hot Start Flex DNA Polymerase (New England Biolabs). The purification of the plasmids was performed using a NucleoBond Xtra Midi kit (Macherey-Nagel). The entire sequences of the WT and mutated plasmids were verified by Sanger sequencing. All primers are listed in Supplemental Table 2.

Cell culture, transfections, and NRG1 stimulation. Neuro-2a cells (RRID:CVCL_0470, ATCC CCL-131) were grown in DMEM (Life Technologies) supplemented with 10% FBS, 100 μg/mL streptomycin, and 100 U/mL penicillin (Life Technologies) at 37°C, 5% CO_2. One hundred nanograms of plasmids carrying WT or mutant hemagglutinin peptide HA-ERBB3 cDNA and 100 ng plasmids carrying WT or mutant HA- or FLAG-tagged ERBB2 cDNA, alone or together, were transfected into Neuro-2a cells in 24-well plates containing coverslips (150,000 cells/well) or in 6-well plates (300,000 cells/well) using Lipofectamine and Plus Reagent (Thermo Fisher Scientific). Forty-eight hours after transfection, cells were fixed in 4% paraformaldehyde or methanol and kept in PBS for subsequent immunohistochemistry experiments. Alternatively, after 48 hours cells were starved in FBS-free DMEM for 2 hours and stimulated for 1 hour at 37°C with 100 ng/mL heregulin (rhNRG1, Cell Signaling Technology). Untreated or treated cultures were subsequently used to perform Western blot experiments.

Immunocytochemistry experiments on transfected Neuro-2a cells. Fixed cells were blocked in PBS with 3% BSA (MilliporeSigma) for 3 hours. Slides were then incubated overnight at 4°C in PBS with 1% BSA and the appropriate antibodies from the following list: anti-HA (Roche Applied Science, clone 12CA5, RRID:AB_514506, mouse, 1/300), anti-FLAG (Merck, F7425, RRID:AB_439687, rabbit, 1/300), Alexa Fluor 488 donkey anti-mouse (Life Technologies, 1/300), and Alexa Fluor 555 donkey anti-rabbit IgG (Life Technologies, 1/300). Briefly, anti-HA or anti-FLAG antibodies were used in combination with Texas Red–X phalloidin (Invitrogen, 1:500) staining. Slides were mounted in Mounting Medium for Fluorescence with DAPI (Vector Laboratories) and examined with a LSM 700 laser scanning confocal microscope (Carl Zeiss) to analyze subcellular localization of ERBB3 and ERBB2. Image analysis and quantification of receptor molecules at the membrane were performed using the ImageJ software.

Western blot. Cells in 6-well plates were washed with ice-cold PBS and harvested in Pierce RIPA buffer containing protease and phosphatase inhibitors (Thermo Fisher Scientific). The total protein levels were determined by bicinchoninic acid (BCA) protein assay using the BCA Protein Assay Kit (Thermo Fisher Scientific). A total of 40 μg protein per sample was run on a polyacrylamide gel and transferred to a PVDF membrane using the Trans-Blot Turbo Transfer System (Bio-Rad).

Phosphorylated ERBB3 and total ERBB3 were detected on the same blots before and after stripping using the following antibodies: anti-P-ERBB3 (Cell Signaling, Y1289 D1B5, rabbit, 1/1000), anti-ERBB3 (Cell Signaling, D22C5, RRID:AB_2721919, 1/1000), and rabbit IgG-HRP and mouse IgG-HRP (Abcam, ab6789, 1/10000). Similar experiments were performed using rabbit P-ERBB2 (Cell Signaling, Y1248, 1/1000) and rabbit ERBB2 (Cell Signaling, 29D8, RRID:AB_10692490, 1/1000) antibodies. Mouse anti-actin beta (Abcam, RRID:AB_306371, 1/2500) was used as a loading control. Blots were visualized using the Amersham ECL Prime Western Blotting Detection Reagent (GE Healthcare), a ChemiDoc XRS+ System and the ImageLab software (Bio-Rad). Note that Neuro-2a cells transfected with empty plasmid were used as negative controls and showed an absence of endogenous ERBB3 and ERBB2 expression (data not shown).

Single-cell RNA-sequencing data sets and analysis. Single-cell RNA-sequencing(sc-RNAseq) data sets were previously published, deposited under accession GSE149524 at Gene Expression Omnibus, and consisted of embryonic ENS isolated from small intestine of *Wnt-1Cre-R26RTomato* mice at E15.5 and E18.5 (68). scRNA-seq data sets were analyzed as previously described (68). Both neuroblasts and differentiating neurons were classified as neurons in Figure 5A.

Statistics. All statistical analyses and graphing were done using R. Data are presented as mean ± SEM in the graphs, and were analyzed using unpaired 2-tailed Student's *t* tests for comparisons of samples with normal distribution, and Mann-Whitney tests for comparisons of samples without assumption of normal distribution. The *P* values were adjusted for multiple comparisons using the Holm-Bonferroni method and presented as follows: NS $P > 0.05$, $^{*}P < 0.05$, $^{**}P < 0.01$, $^{***}P < 0.001$.

Study approval. This research received a favorable opinion from the Ethics Committee of Paris Ile-de-France II (2015-03-03). Written informed consent to participate in biomedical research was obtained from the legal representative(s) of all patients. Animal studies were conducted in accordance with the guidelines issued by the French Ministry of Agriculture and were approved by the Direction Départementale des Services Vétérinaires de Paris.

Author contributions

TLL, SL, JA, and NB conceived the study and its design. TLL, JL, PS, DMEIH, AP, SD, CBF, PN, SW, RH, BK, CTG, and JA analyzed and interpreted the genetic data. TLL, LG, ML, JM, AG, FG, AC, TJM, and NB analyzed and interpreted the histopathology. PS, CG, MH, OG, CC, YC, LM, HEB, TJM, AB, ACT, BK, HJMS, IFMD, SL, and JA performed clinical evaluation. TLL, TEJT, HJMS, CTG, JA, and NB performed in silico and in vitro functional analyses and data interpretation. TLL, FB, and NB analyzed mouse models. KM and UM analyzed scRNA-seq data. TLL, JA, and NB drafted the manuscript. LG, UM, and CTG performed critical revision of the manuscript. All authors approved the final version of the manuscript.

Acknowledgments

The authors thank the families and their medical referents for participation in the study; Lindsey Oudijk, Marie-Christine Fuseau, Nathalie Yvart, and members of the SFR Necker histology platform for technical help; ARCC for the slide scanner; Sylvain Ernest for advice on plasmid manipulation; Lisa Zerad for help during mouse studies; members of the SFR Necker Cell Imaging platform for advice on image acquisition and analysis; Megan Cho for scientific networking; Mara P. Steinkamp for providing the WT *ERBB2* and *ERBB3* tagged constructs; Carmen Birchmeier for providing the *ErbB3* mutant mouse strain; Jean-François Brunet for access to *ErbB3* mutant mice and for comments on the manuscript; and members of the International HSCR Consortium. This work was supported by the Institut National de la Santé et de la Recherche Médicale (INSERM), state funding from the Agence Nationale de la Recherche under the "Investissements d'avenir" program (ANR-10-IAHU-01), the MSD-Avenir fund (DEVO–DECODE project), the Association Francophone de la Maladie de Hirschsprung (AFMAH) and the Association Rires et tapage chez les Hirschsprung. TLL received fellowships from the French Embassy in Vietnam and the Fondation pour la Recherche Médicale (FDT201904008113).

Address correspondence to: Jeanne Amiel or Nadège Bondurand, UMR-1163 INSERM, Institut Imagine, Laboratoire d'Embryologie et Génétique des Malformations, 24 Boulevard du Montparnasse F-75015, Paris, France. Phone: 33.14.275.4326; Email: jeanne.amiel@inserm.fr (JA); nadege.bondurand@inserm.fr (NB).

1. Hirschsprung H. Stuhlträgheit neugeborener in folge von dilatation und hypertrophie des colons. *Jahrbuch Kinderheilkunde Physische Erziehung*. 1888;27:1–7.
2. Amiel J, et al. Hirschsprung disease, associated syndromes and genetics: a review. *J Med Genet*. 2008;45(1):1–14.
3. Heuckeroth RO. Hirschsprung disease - integrating basic science and clinical medicine to improve outcomes. *Nat Rev Gastroenterol Hepatol*. 2018;15(3):152–167.
4. Bodian M, et al. Hirschsprung's disease and idiopathic megacolon. *Lancet*. 1949;1(6540):6–11.
5. Edery P, et al. Mutations of the RET proto-oncogene in Hirschsprung's disease. *Nature*. 1994;367(6461):378–380.
6. Attié T, et al. Diversity of RET proto-oncogene mutations in familial and sporadic Hirschsprung disease. *Hum Mol Genet*. 1995;4(8):1381–1386.
7. Angrist M, et al. Mutation analysis of the RET receptor tyrosine kinase in Hirschsprung disease. *Hum Mol Genet*. 1995;4(5):821–830.
8. Emison ES, et al. A common sex-dependent mutation in a RET enhancer underlies Hirschsprung disease risk. *Nature*. 2005;434(7035):857–863.
9. Emison ES, et al. Differential contributions of rare and common, coding and noncoding Ret mutations to multifactorial Hirschsprung disease liability. *Am J Hum Genet*. 2010;87(1):60–74.
10. Tilghman JM, et al. Molecular genetic anatomy and risk profile of Hirschsprung's disease. *N Engl J Med*. 2019;380(15):1421–1432.
11. Anuras S, et al. Intestinal pseudoobstruction. *Gastroenterology*. 1978;74(6):1318–1324.
12. Brosens E, et al. Genetics of enteric neuropathies. *Dev Biol*. 2016;417(2):198–208.
13. Gargiulo A, et al. Filamin A is mutated in X-linked chronic idiopathic intestinal pseudo-obstruction with central nervous system involvement. *Am J Hum Genet*. 2007;80(4):751–758.
14. Kapur RP, et al. Diffuse abnormal layering of small intestinal smooth muscle is present in patients with FLNA mutations and x-linked intestinal pseudo-obstruction. *Am J Surg Pathol*. 2010;34(10):1528–1543.
15. Mungan Z, et al. Familial visceral myopathy with pseudo-obstruction, megaduodenum, Barrett's esophagus, and cardiac abnormalities. *Am J Gastroenterol*. 2003;98(11):2556–2560.
16. Bonora E, et al. Mutations in RAD21 disrupt regulation of APOB in patients with chronic intestinal pseudo-obstruction. *Gastroenterology*. 2015;148(4):771–782.
17. Chetaille P, et al. Mutations in SGOL1 cause a novel cohesinopathy affecting heart and gut rhythm. *Nat Genet*. 2014;46(11):1245–1249.

18. Lehtonen HJ, et al. Segregation of a missense variant in enteric smooth muscle actin γ-2 with autosomal dominant familial visceral myopathy. *Gastroenterology*. 2012;143(6):1482–1491.
19. Dong W, et al. Identification of a dominant MYH11 causal variant in chronic intestinal pseudo-obstruction: Results of whole-exome sequencing. *Clin Genet*. 2019;96(5):473–477.
20. Yarden Y, Sliwkowski MX. Untangling the ErbB signalling network. *Nat Rev Mol Cell Biol*. 2001;2(2):127–137.
21. Citri A, Yarden Y. EGF-ERBB signalling: towards the systems level. *Nat Rev Mol Cell Biol*. 2006;7(7):505–516.
22. Hynes NE, Lane HA. ERBB receptors and cancer: the complexity of targeted inhibitors. *Nat Rev Cancer*. 2005;5(5):341–354.
23. Dinsmore CJ, Soriano P. MAPK and PI3K signaling: at the crossroads of neural crest development. *Dev Biol*. 2018;444 Suppl 1:S79–S97.
24. Meyer D, et al. Isoform-specific expression and function of neuregulin. *Development*. 1997;124(18):3575–3586.
25. Baselga J, Swain SM. Novel anticancer targets: revisiting ERBB2 and discovering ERBB3. *Nat Rev Cancer*. 2009;9(7):463–475.
26. Hyman DM, et al. HER kinase inhibition in patients with HER2- and HER3-mutant cancers. *Nature*. 2018;554(7691):189–194.
27. Kiavue N, et al. ERBB3 mutations in cancer: biological aspects, prevalence and therapeutics. *Oncogene*. 2020;39(3):487–502.
28. Braunstein EM, et al. A germline ERBB3 variant is a candidate for predisposition to erythroid MDS/erythroleukemia. *Leukemia*. 2016;30(11):2242–2245.
29. Landau D, et al. A new autosomal recessive congenital contractural syndrome in an Israeli Bedouin kindred. *Am J Med Genet A*. 2003;117A(1):37–40.
30. Narkis G, et al. Homozygosity mapping of lethal congenital contractural syndrome type 2 (LCCS2) to a 6 cM interval on chromosome 12q13. *Am J Med Genet A*. 2004;130A(3):272–276.
31. Narkis G, et al. Lethal congenital contractural syndrome type 2 (LCCS2) is caused by a mutation in ERBB3 (Her3), a modulator of the phosphatidylinositol-3-kinase/Akt pathway. *Am J Hum Genet*. 2007;81(3):589–595.
32. Alfares A, et al. A multicenter clinical exome study in unselected cohorts from a consanguineous population of Saudi Arabia demonstrated a high diagnostic yield. *Mol Genet Metab*. 2017;121(2):91–95.
33. Li N, et al. Biallelic ERBB3 loss-of-function variants are associated with a novel multisystem syndrome without congenital contracture. *Orphanet J Rare Dis*. 2019;14(1):265.
34. Tang CS-M, et al. Identification of genes associated with Hirschsprung disease, based on whole-genome sequence analysis, and potential effects on enteric nervous system development. *Gastroenterology*. 2018;155(6):1908–1922.
35. Tang CS, et al. Uncovering the genetic lesions underlying the most severe form of Hirschsprung disease by whole-genome sequencing. *Eur J Hum Genet*. 2018;26(6):818–826.
36. Garcia-Barcelo M-M, et al. Genome-wide association study identifies NRG1 as a susceptibility locus for Hirschsprung's disease. *Proc Natl Acad Sci U S A*. 2009;106(8):2694–2699.
37. Tang CS-M, et al. Mutations in the NRG1 gene are associated with Hirschsprung disease. *Hum Genet*. 2012;131(1):67–76.
38. Luzón-Toro B, et al. Comprehensive analysis of NRG1 common and rare variants in Hirschsprung patients. *PLoS One*. 2012;7(5):36524.
39. Gui H, et al. RET and NRG1 interplay in Hirschsprung disease. *Hum Genet*. 2013;132(5):591–600.
40. Meyer D, Birchmeier C. Multiple essential functions of neuregulin in development. *Nature*. 1995;378(6555):386–390.
41. Lee KF, et al. Requirement for neuregulin receptor erbB2 in neural and cardiac development. *Nature*. 1995;378(6555):394–398.
42. Woldeyesus MT, et al. Peripheral nervous system defects in erbB2 mutants following genetic rescue of heart development. *Genes Dev*. 1999;13(19):2538–2548.
43. Riethmacher D, et al. Severe neuropathies in mice with targeted mutations in the ErbB3 receptor. *Nature*. 1997;389(6652):725–730.
44. Espinosa-Medina I, et al. Dual origin of enteric neurons in vagal Schwann cell precursors and the sympathetic neural crest. *Proc Natl Acad Sci U S A*. 2017;114(45):11980–11985.
45. Gamba E, et al. Deficient alpha smooth muscle actin expression as a cause of intestinal pseudo-obstruction: fact or fiction? *J Clin Pathol*. 2004;57(11):1168–1171.
46. Knowles CH, et al. The London classification of gastrointestinal neuromuscular pathology: report on behalf of the Gastro 2009 International Working Group. *Gut*. 2010;59(7):882–887.
47. Chalazonitis A, et al. Bone morphogenetic proteins regulate enteric gliogenesis by modulating ErbB3 signaling. *Dev Biol*. 2011;350(1):64–79.
48. Barrenschee M, et al. Expression and function of Neuregulin 1 and its signaling system ERBB2/3 in the enteric nervous system. *Front Cell Neurosci*. 2015;9:360.
49. Czerwinski M, et al. In vitro and in vivo development of the human intestinal niche at single cell resolution [published online February 1, 2020]. *bioRxiv*. https://doi.org/10.1016/j.stem.2020.11.008.
50. Schulze WX, et al. Phosphotyrosine interactome of the ErbB-receptor kinase family. *Mol Syst Biol*. 2005;1:2005.0008.
51. Pingault V, et al. SOX10 mutations in patients with Waardenburg-Hirschsprung disease. *Nat Genet*. 1998;18(2):171–173.
52. Pingault V, et al. Review and update of mutations causing Waardenburg syndrome. *Hum Mutat*. 2010;31(4):391–406.
53. Pingault V, et al. Peripheral neuropathy with hypomyelination, chronic intestinal pseudo-obstruction and deafness: a developmental "neural crest syndrome" related to a SOX10 mutation. *Ann Neurol*. 2000;48(4):671–676.
54. Pingault V, et al. SOX10 mutations in chronic intestinal pseudo-obstruction suggest a complex physiopathological mechanism. *Hum Genet*. 2002;111(2):198–206.
55. Hogan AR, et al. Waardenburg syndrome type IV de novo *SOX10* variant causing chronic intestinal pseudo-obstruction. *Pediatr Gastroenterol Hepatol Nutr*. 2019;22(5):487–492.
56. Faure S, et al. Enteric neural crest cells regulate vertebrate stomach patterning and differentiation. *Development*. 2015;142(2):331–342.
57. Graham HK, et al. Intestinal smooth muscle is required for patterning the enteric nervous system. *J Anat*. 2017;230(4):567–574.
58. Bourret A, et al. Colonic mesenchyme differentiates into smooth muscle before its colonization by vagal enteric neural crest-derived cells in the chick embryo. *Cell Tissue Res*. 2017;368(3):503–511.
59. Duchesne M, et al. Assessing sudomotor impairment in patients with peripheral neuropathy: comparison between electrochemical skin conductance and skin biopsy. *Clin Neurophysiol*. 2018;129(7):1341–1348.
60. Romero NB, et al. Main steps of skeletal muscle development in the human: morphological analysis and ultrastructural characteristics of developing human muscle. *Handb Clin Neurol*. 2013;113:1299–1310.
61. Jungbluth H, et al. Congenital myopathies: disorders of excitation-contraction coupling and muscle contraction. *Nat Rev Neurol*. 2018;14(3):151–167.
62. Van Ho AT, et al. Neural crest cell lineage restricts skeletal muscle progenitor cell differentiation through Neuregulin1-ErbB3 signaling. *Dev Cell*. 2011;21(2):273–287.
63. Hicks MR, et al. ERBB3 and NGFR mark a distinct skeletal muscle progenitor cell in human development and hPSCs. *Nat Cell Biol*. 2018;20(1):46–57.
64. Le T-L, et al. Bi-allelic variations of SMO in humans cause a broad spectrum of developmental anomalies due to abnormal hedgehog signaling. *Am J Hum Genet*. 2020;106(6):779–792.
65. Jura N, et al. Structural analysis of the catalytically inactive kinase domain of the human EGF receptor 3. *Proc Natl Acad Sci U S A*. 2009;106(51):21608–21613.
66. Aertgeerts K, et al. Structural analysis of the mechanism of inhibition and allosteric activation of the kinase domain of HER2 protein. *J Biol Chem*. 2011;286(21):18756–18765.
67. Steinkamp MP, et al. erbB3 is an active tyrosine kinase capable of homo- and heterointeractions. *Mol Cell Biol*. 2014;34(6):965–977.
68. Morarach K, Mikhailova A, Knoflach V, et al. Diversification of molecularly defined myenteric neuron classes revealed by single-cell RNA sequencing. *Nat Neurosci*. 2021;24(1):34–46.